Received: 12 January 2019 | Revised: 9 April 2021 | Accepted: 29 April 2021

DOI: 10.1111/jmg.12610

ORIGINAL ARTICLE

Journal of METAMORPHIC GEOLOGY WILEY

Partially open grain and phase boundaries as fluid pathways in metamorphic and magmatic rocks

Richard Wirth[1] | **Jörn H. Kruhl**[2,4] | **Luiz F. G. Morales**[3] | **Anja Schreiber**[1]

[1]Helmholtz Centre Potsdam, GFZ German Research Centre for Geosciences, Potsdam, Germany

[2]Department of Earth and Environmental Sciences, Ludwig-Maximilians-Universität München, Munich, Germany

[3]Scientific Center for Optical and Electron Microscopy (ScopeM), Zürich, Switzerland

[4]Faculty of Civil, Geo and Environmental Engineering, Technische Universität München, Munich, Germany

Correspondence
Jörn H. Kruhl, Department of Earth and Environmental Sciences, Ludwig-Maximilians-Universität München, Theresienstr. 41, 80333 Munich, Germany.
Email: kruhl@tum.de

Funding information
Deutsche Forschungsgemeinschaft, Grant/Award Number: KR691/36-1 / SCHM390/17-1

Handling Editor: Bernardo Cesare

Abstract

Transmission electron microscopy and 3D focused ion beam/scanning electron microscope nanotomography are applied to grain and phase boundaries between quartz, plagioclase, K-feldspar, clinopyroxene, amphibole, and calcite. The samples come from metamorphic, plutonic and volcanic rocks, and hydrothermal quartz, and experienced cooling and decompression after highly variable *P–T* peak conditions. Most of the boundaries are partially open in the range of up to several hundred nanometres and partly to totally filled with secondary minerals, such as actinolite, biotite, chlorite, sheet silicates, and quartz, as well as with amorphous matter. Cracking and opening of boundaries are suggested to be related to anisotropic thermoelastic response of crystals to cooling. It starts below the brittle–ductile transition of the involved minerals. The partially open grain and phase boundaries, together with dissolution-generated cavities, can form porosity of more than 2 vol.% and permeability under conditions of at least lowermost greenschist facies. Such networks of partially open or partially refilled boundaries potentially affect properties of crystalline rocks and processes in the upper crust, such as metasomatism, weathering, migration of radionuclides through bedrock of geological repositories of nuclear waste, and deformation in nature and in experiment.

KEYWORDS

fluid pathways, focused iron beam technique, partially open grain and phase boundaries, transmission electron microscopy

1 | INTRODUCTION

Grain and phase boundaries, especially synthetic grain boundaries, are generally regarded as dense, non-permeable structures (Etheridge et al., 1983; Hay & Evans, 1988; Heinemann et al., 2001, 2005; Marquardt et al., 2010). However, pores along grain boundaries in metamorphic rocks have been illustrated by scanning electron microscopy (SEM) (Mancktelow et al., 1998; Mancktelow & Pennacchioni, 2004) and the existence of nanometre-wide channels along three-grain junctions (triple lines) in experiments has been verified (Lee et al., 1991; Watson & Brenan, 1987). Such channels are considered as fluid pathways (Price et al., 2006; Schenk & Urai, 2004). Fluid migration appears to occur transiently in pulses (Beinlich et al., 2020; John et al., 2012; Plümper et al., 2017) generated by episodic increase in pore fluid pressure (Taetz et al., 2018). Such pulses are related to (a) fault rupture events (Cox, 2007; Taetz et al., 2018),

(b) the formation of networks of microfractures (Jamtveit et al., 2008), and (c) fracturing along grain boundaries (Shimizu et al., 2017). Basically, these investigations provide arguments that open grain boundaries as well as microfractures in rocks of the lower and middle crust and of subducting slabs may lead to transient permeability over geologically short periods. However, they do not show that grain boundaries and microfractures are open and permeable over geologically longer periods.

Recently, transmission electron microscopy (TEM), based on focused ion beam (FIB) prepared samples, together with FIB/SEM nanotomography evidenced that quartz grain boundaries in metamorphic rocks are partially open with widths of up to several hundred nanometres and form a network that serves as pathway for fluids (Kruhl et al., 2013). Opening is considered as the result of cooling-induced anisotropic volume reduction during uplift and below the approximate temperature threshold for dislocation creep ('brittle-ductile transition'; Nicolas & Poirier, 1976). This threshold is equivalent to the recrystallization temperature, which is for example ~300°C for quartz (Stipp et al., 2002; Stöckhert et al., 1999; Voll, 1976). The volume reduction is not totally balanced by decompression-induced anisotropic volume expansion. The degree of measured grain-boundary opening is roughly in agreement with semi-quantitative modelling, which indicates that, due to temperature–pressure-related volume change, at least 50% of the total grain-boundary area is open (Kruhl et al., 2013).

In the present study, we expand the previous investigation to grain and phase boundaries of various rock-forming minerals—calcite, quartz, plagioclase, K-feldspar, amphibole, and clinopyroxene—from volcanic, plutonic, and metamorphic rocks as well as from hydrothermal quartz. We studied seven different samples from seven different environments via TEM and FIB/SEM. We document the widespread existence of partially open grain and phase boundaries in natural rocks—probably partly already open under greenschist facies conditions and over geologically longer periods.

2 | METHODS

Investigations were performed based on polarized-light microscopy, FIB sample preparation, FIB-SEM tomography, and TEM. First, we selected grain and phase boundaries of minerals of interest in uncovered thin sections, relatively steep to the thin-section surface and mainly without visible alteration products. In general, we tried to select boundaries that appeared 'closed' under the polarized-light microscope. Subsequently, TEM foils were prepared or FIB/SEM was used for 3D imaging. For each sample, boundaries in 1–2-mm sized areas of one thin section were analysed. Consequently, distances between these boundaries are in the range of several hundred μm to 1–2 cm as a maximum.

We have to emphasize that FIB sample preparation or the FIB/SEM nanotomography technique do not introduce artefacts like cracks or cavities to the specimen. Sample preparation definitely does not produce any of the features of the studied grain boundaries described here. This was already discussed in detail in a previous paper on partially open quartz grain boundaries (Kruhl et al., 2013). Additionally, this is based on the experience of more than 6,000 TEM foils sputtered with FIB from different materials and studied with TEM by one of the authors (RW).

Transmission electron microscopy was performed with a Tecnai F20 X-twin TEM with a Schottky field emitter as electron source. The TEM is equipped with a Gatan Tridiem Imaging Filter GIF, a Fishione high-angle annular dark field (HAADF) detector operated at a camera length (330 mm) that allows Z-contrast plus diffraction contrast imaging, and an EDAX X-Ray analyser. EDX analyses were generally performed in the scanning transmission mode (STEM) to avoid beam damage. Usually, acquisition time was 60 s and bright field images were acquired as energy filtered images applying a 20 eV window to the zero loss peak. Calcite and quartz are very sensitive to electron irradiation damage. Consequently, at lower magnification images were generally acquired in the scanning transmission mode as HAADF images, thus reducing the irradiation damage substantially. Most of the grain and phase boundary images, bright field as well as HAADF images, show the perforated carbon film, on which the FIB prepared membrane rests, as shadow image.

In total, 43 grain and phase boundaries between six different types of minerals, and four fractures and one cleavage plane are analysed with the HRTEM-FIB method. These boundaries and planes represent the total amount of analysed material. In other words, we present the data from all HRTEM-FIB foils prepared from seven rock samples. The foils are oriented approximately perpendicular to the thin-section surface and to the grain or phase boundary (Figure 1a). Their observable lengths range from ~3 to 12 μm, with the majority ~8–9 μm (Table S1). Lengths of boundaries, cleavage planes, and fractures add to ~380 μm. Lengths, opening widths, and areas of cavities are measured in TEM images (Figure 1b). Determination of cavity areas is slightly inaccurate if cavity boundaries are oriented obliquely to the TEM foil. The porosity of open boundaries and cavities is determined as percentage of area. Because the sample fabrics are roughly isotropic it appears justified to equate these values with volume percentage.

Grain diameters are measured under the polarized-light microscope. Because these measurements can only be performed in 2D they may be fraught with large errors.

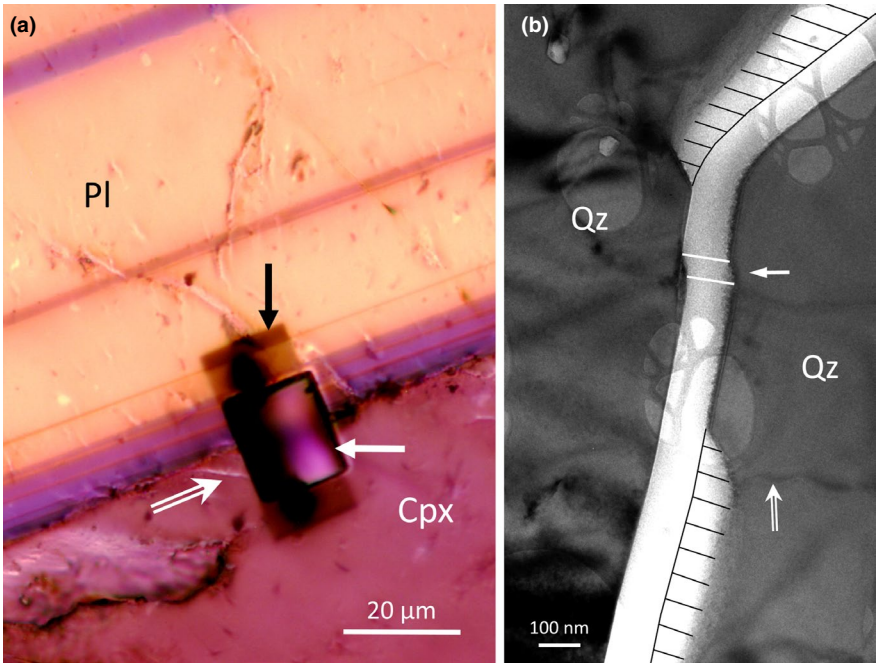

FIGURE 1 (a) Site of foil preparation in thin section across a plagioclase–clinopyroxene phase boundary. The dark-rimmed rectangle (white arrow) marks the excavated pit, from which the foil was taken. Redeposited material forms a darker, rectangular area (black arrow). The dark stripe within this area is caused by relics of platinum. The white double arrow indicates the direction of view perpendicular to the foil shown in Figure 6. The albite deformation twins in plagioclase (parallel, thin lamellae) are also clearly visible in the HAADF TEM image (Figure 6). Sample KR3238B; foil 4843; photomicrograph with crossed polars and lambda plate inserted. (b) Weakly segmented, ~100 nm open quartz grain boundary, with opposing crystal faces strictly parallel to each other. A kink (arrow) indicates an opening direction nearly perpendicular to the lower part of the boundary. Local enlargements of the open boundary (fasciated areas) are partly developed where lattice defects (double arrow) meet the crystal faces. The enlargements have crystallographically controlled straight margins and are interpreted as dissolution–precipitation cavities. Hydrothermal quartz; sample KR5095A, foil 4836 [Colour figure can be viewed at wileyonlinelibrary.com]

Consequently, such errors falsify, for example, grain-size related correlations. Minerals on grain scale are identified under the polarized-light microscope. Fillings of open grain and phase boundaries and of cavities are determined, based on their textures, on semi-quantitative TEM EDX analyses, and on diffraction data.

3 | SAMPLES, OBSERVATIONS, AND MEASUREMENTS

The analysed rocks come from different regions with different *P*–*T*-deformation histories (Figure 2): (a) jadeite quartzite from the ultra high pressure region of Dabie Shan (Central Eastern China), (b) metagabbro and Cpx-granulite from the lower and middle part of the fossil Variscan lower continental crust of Calabria (Southern Italy), (c) Carrara marble from the medium-grade metamorphic Apennine nappes of Tuscany (Italy), (d) amphibole monzonite from the Joshua Flat Pluton (White-Inyo Mountains, California), (e) tholeiitic basalt from the Hegau (Germany), and (f) hydrothermal quartz from the post-Variscan brittle Pfahl shear zone (Bavarian Forest, Germany).

3.1 | Jadeite quartzite (sample RP11)

Larger parts of the Dabie–Sulu Belt (Central Eastern China) were subducted to the upper mantle at 236 ± 32 Ma (Ayers et al., 2002), and obducted forming kilometre large bodies of eclogite and jadeite quartzite. The sample originates from the Shuanghe region, experienced peak *P*–*T* conditions of ~30 kbar and 650°C, and reached ~550°C and 7 kbar during retrograde development (Figure 2; Su et al., 1996). It is composed of millimetre-sized jadeite, garnet, and quartz (Figure 3a). Albite–amphibole symplectite between jadeite and quartz most probably formed at $P < 8$ kbar and $T < 550$°C (Liou et al., 1997).

The nine analysed boundaries between albite, quartz, amphibole, and jadeite, and one crack in amphibole, with total length of 87.6 µm (Table S1), are partly open up to 450 nm (Table 1). Larger cavities of variable size are common (Figure 4). Steps along straight boundary segments are crystallographically controlled and mostly reach into albite. Sheet silicate and occasionally opaque matter fill the quartz–amphibole and albite–jadeite phase boundaries, a crack in amphibole, and the dissolution cavities (Figure S1). Rarely, sheet silicate replaces amphibole or jadeite but mostly fills the already open boundaries and

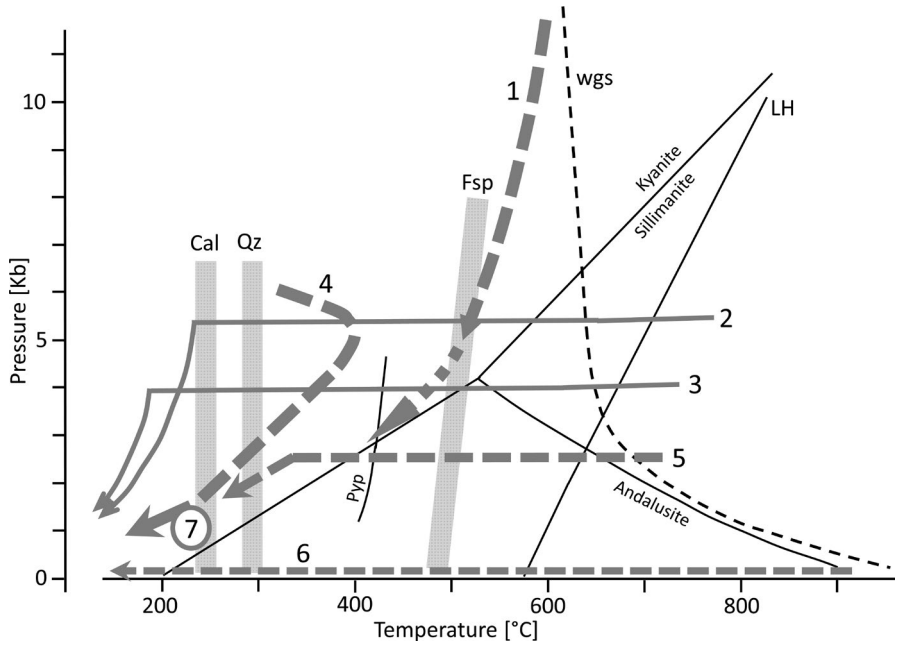

FIGURE 2 *P–T* diagram with cooling–decompression paths of the analysed samples. Stability fields of Al_2SiO_5 polymorphs after Bohlen et al. (1991); upper stability limit of pyrophyllite (Pyp) after Kerrick (1968); wet granite solidus (wgs) after Huang and Wyllie (1981); low–high quartz transition (LH) after Gross and Van Heege (1971); approximate temperature threshold for dislocation creep ('brittle-ductile transition'; Nicolas & Poirier, 1976) of various minerals, equivalent to recrystallization temperatures, with an uncertainty of ±10–15°C: Cal (Burkhard, 1993), Qz (Stipp et al., 2002; Stöckhert et al., 1999; Voll, 1976), Fsp (Pl and Kf Altenberger et al., 1987; Kruhl, 1993; Tullis, 1983; Voll, 1976). *P–T* paths of analysed samples: 1—jadeite quartzite from the Shuanghe region (Dabie Shan, China); 2 and 3—metagabbro and Cpx-granulite from the fossil Variscan lower continental crust of Calabria; 4—calcite marble from the Alpi Apuane (Carrara, Tuscany/Italy); 5—amphibole monzonite from the Joshua Flat Pluton (White-Inyo Mountains, California); 6—Tholeiitic basalt from the Hegau volcanic area (southern Germany); 7—Hydrothermal quartz from the Bavarian Pfahl shear zone

cavities, indicated by variable orientation of layers (Figure 5). In contrast, grain boundaries between quartz grains do not contain any filling (Table 1). The boundaries between grains and sheet-silicate filling are partly open up to ~100 nm, although single layers are locally offset or attached to quartz (Figure 5b). The average volume of open/filled boundaries and cavities adds to ~0.13% and ~0.07% (Table 1).

3.2 | Metagabbro (sample KR3238B)

The sample originates from the exposed lowermost part of the fossil Variscan lower continental crust of Calabria (southern Italy) and experienced peak metamorphism of ~750 to 800°C and 7.5 kbar (Schenk, 1989). It is composed of mainly plagioclase, amphibole, and clinopyroxene (Figure 3b). Subsequent uplift by ~7 km led to slow post-Variscan cooling at 5.5 kbar (Figure 2). Annealed fabrics and granulite facies parageneses show that the analysed sample did not experience deformation or retrograde metamorphism during cooling.

Nine phase boundaries between plagioclase (bytownite), clinopyroxene, and amphibole, and two fractures and one cleavage plane in amphibole, with a total length of 73.5 μm (Table S1), were analysed. All of them are open in the range of several hundred nanometres (Table 1), with cavities of >2 μm width. They are mostly filled with sheet silicate flakes of variable orientation (Figure 6) but also with actinolite, identified by electron diffraction, and subhedral, micrometre-small quartz (Figure 7). The opposing crystal faces form crystallographically controlled dissolution steps or straight segments parallel to twin boundaries in plagioclase (Figure 6). The average volume of filled boundaries and cavities adds to ~0.42% and ~0.13% (Table 1).

3.3 | Cpx-granulite (sample KR3434B)

The sample originates from the exposed medium part of the fossil Variscan lower continental crust of Calabria. It experienced peak metamorphism of ~700–750°C and 6 kbar (Schenk, 1989). Subsequent uplift by ~7 km led to slow cooling at 4 kbar (Figure 2). The sample is composed of mainly plagioclase, quartz, and clinopyroxene (Figure 3c). Preserved granulite facies parageneses with annealed fabrics indicate that the sample did not experience deformation or retrograde metamorphism during isobaric cooling and exhumation. On the regional scale, retrograde deformation concentrated in discrete shear zones, however, decametres away from the sample site.

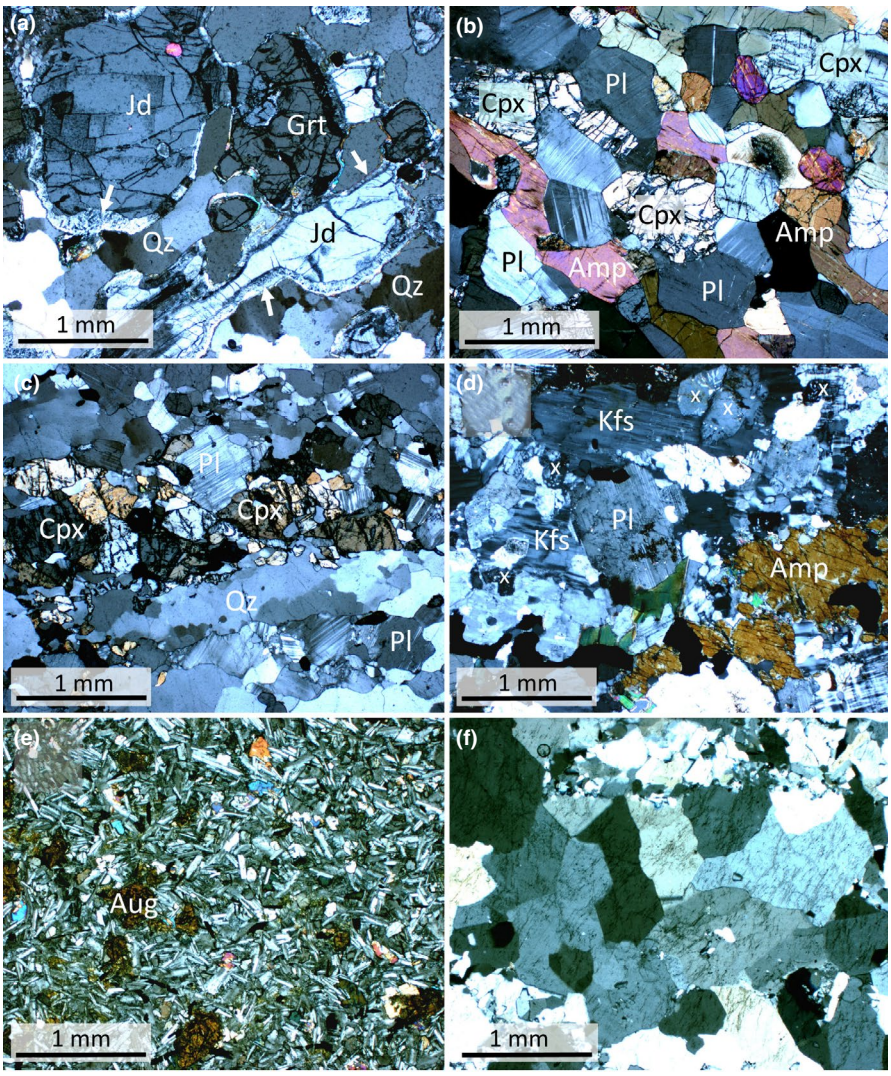

FIGURE 3 Microfabrics of analysed samples; photomicrographs with crossed polars. (a) Jadeite quartzite with millimetre-sized jadeite (Jd), garnet (Grt), quartz (Qz) and albite–amphibole symplectite between jadeite and quartz (white arrows). (b) Metagabbro with ~0.5–1 mm-sized, polygonal, slightly elongate grains of plagioclase (Pl), amphibole (Amp), and clinopyroxene (Cpx). Alignment of grains represents the granulite facies foliation. (c) Cpx-granulite with ~0.1–1 mm-sized plagioclase (Pl), quartz (Qz) and clinopyroxene (Cpx). Ribbons of these minerals form the granulite facies foliation. (d) Amphibole monzonite with millimetre-sized plagioclase (Pl), K-feldspar (Kfs), amphibole (Amp), quartz, and biotite. Kfs is partly replaced by myrmekite (x). (e) Tholeiitic basalt with randomly oriented, ~100–200 μm long, thin-tabular, twinned plagioclase; augite (Aug) and olivine (coloured, xenomorph grains). (f) Polygonal, millimetre-sized, hydrothermal quartz with networks of fluid inclusion patches [Colour figure can be viewed at wileyonlinelibrary.com]

Five phase boundaries between quartz and clinopyroxene and one fracture in clinopyroxene, with a total length of ~52 μm (Table S1), were analysed. Before filling, they were open in the range of several hundred nanometres but mostly without larger cavities (Figure 8a). Boundaries and fractures are filled with sheet silicate (probably vermiculite). Amorphous matter exists in central parts of open clinopyroxene grain boundaries. It is accompanied on both sides by sheet silicate (Figure 8b). The boundaries between the two materials show geometrically fitting, opposing steps. Sheet silicate replaces clinopyroxene along crystallographic planes as well as planar arrangements of lattice defects. The average volume of filled boundaries and the crack adds to ~0.33% and ~0.11% (Table 1).

3.4 | Calcite marble (sample W238)

The sample represents a virtually pure calcite marble from the Alpi Apuane (Carrara, Tuscany/Italy). During Alpine (Tertiary) orogeny, it experienced maximum temperatures and pressures of 400°C and ~6 kbar (Figure 2; Franceschelli et al., 1997; Kligfield et al., 1986).

The three analysed grain boundaries, with a total length of ~23 μm (Table S1), are open in the range of 40–180 nm (Table 1) and accompanied by cavities of similar width. These cavities formed, where dislocations meet grain faces (Figure 9). The cavity boundaries are segmented and strictly follow three different, probably crystallographically controlled orientations. Filling of the open boundaries with secondary minerals was not observed. The average volume of open boundaries and cavities adds to ~0.41% and ~0.29% (Table 1).

3.5 | Amphibole monzonite (sample KR3720)

The sample is composed of mainly plagioclase, K-feldspar, and amphibole (Figure 3d). It was taken from the

TABLE 1 Characteristics of analysed grain and phase boundaries as well as cracks and one cleavage plane

Sample/foil number	Mineral 1	Mineral 2	Opening width of crack or boundary (μm)	Area of open/filled crack or boundary ($μm^2$)	Area of dissolution cavity ($μm^2$)	Filling of open grain and phase boundaries, cracks and cavities	Average grain diameter (μm)	Average vol.% of open/filled crack or boundary	Average vol.% of dissolution cavity	Average total porosity (vol.%)
RP11/3344	Quartz	Quartz	0.455	3.912	0.02605	Open	239	0.13345	0.07129	0.20474
RP11/3346	Quartz	Quartz	0.200	1.626	0.00000	Open				
RP11/3346	Quartz	Quartz	—	0.000	—	Closed				
RP11/3348	Quartz	Quartz	0.440	3.657	1.63397	Open				
RP11/4838	Amphibole	Quartz	0.250	2.435	4.00616	Vermiculite (?)				
RP11/4838	Albite	Amphibole	—	0.000	—	Closed				
RP11/4838	Crack in amphibole		0.100	0.610	0.80483	Vermiculite (?)				
RP11/4840	Albite	Jadeite	0.050	0.357	0.82074	Ilmenite				
RP11/4840	Albite	Albite	0.057	0.304	0.00000	Open				
RP11/4842	Albite	Jadeite	0.110	1.057	0.17010	Open, sheet silicate				
KR3238B/2877	Amphibole	Amphibole	0.425	2.333	0.00000	Sheet silicate	131	0.42498	0.12899	0.55397
KR3238B/2880	Bytownite	Amphibole	nd	—	nd	Quartz, sheet silicate				
KR3238B/4841	Amphibole	Amphibole	0.580	4.444	0.00000	Actinolite (?)				
KR3238B/4841	Cleavage in amphibole		0.250	1.688	0.00000	Actinolite (?)				
KR3238B/4843	Bytownite	Diopside	0.300	2.299	0.50295	Sheet silicate				
KR3238B/4846	Diopside	Diopside	0.145	1.168	0.37519	Actinolite (?)				
KR3238B/5832	Plagioclase	Amphibole	0.264	2.320	4.00354	Sheet silicate, quartz				
KR3238B/5833	Amphibole	Amphibole	0.234	2.838	0.00000	Sheet silicate				
KR3238B/5833	Crack in amphibole		0.213	2.248	0.00000	Sheet silicate				
KR3238B/5834	Plagioclase	Amphibole	nd	—	—	Sheet silicate				
KR3238B/5835	Plagioclase	Amphibole	0.042	0.336	1.14878	Sheet silicate, albite				
KR3238B/5835	Crack in amphibole		0.091	0.273	0.10935	Sheet silicate				
KR3434B/4833	Crack in diopside		0.455	3.545	0.00000	Sheet silicate	218	0.32753	0.11338	0.44091
KR3434B/4835	Diopside	Diopside	0.610	4.516	0.30612	Sheet silicate, amorphous matter				
KR3434B/4837	Diopside	Diopside	0.500	4.481	1.88272	Vermiculite (?)				
KR3434B/5829	Quartz	Diopside	0.261	2.664	1.80611	Sheet silicate				
KR3434B/5830	Quartz	Diopside	0.252	2.356	2.03482	Sheet silicate				
KR3434B/5831	Diopside	Diopside	0.124	1.041	0.40962	Sheet silicate				
W238/2766	Calcite	Calcite	0.182	1.713	0.89453	Open	59	0.41278	0.29129	0.70407
W238/2769	Calcite	Calcite	0.120	0.847	0.42438	Open				
W238/2771	Calcite	Calcite	0.040	0.271	0.67885	Open				

(Continues)

TABLE 1 (Continued)

Sample/foil number	Mineral 1	Mineral 2	Opening width of crack or boundary (μm)	Area of open/filled crack or boundary (μm^2)	Area of dissolution cavity (μm^2)	Filling of open grain and phase boundaries, cracks and cavities	Average grain diameter (μm)	Average vol.% of open/filled crack or boundary	Average vol.% of dissolution cavity	Average total porosity (vol.%)
KR3720/2876	Plagioclase	Amphibole	0.275	2.966	2.04058	Open, biotite	66	0.93550	0.32550	1.26100
KR3720/2881	K-feldspar	Quartz	0.305	2.093	0.00000	Open, quartz (?)				
KR3720/2881	Amphibole	Quartz	0.365	2.469	0.57870	Open, amphibole, sheet silicate				
KRM51/3347	Plagioclase	Plagioclase	0.108	0.849	0.25477	Sheet silicate	39	0.79672	1.35979	2.15651
KRM51/3355	Plagioclase	Plagioclase	0.030	0.142	2.29132	Sheet silicate				
KRM51/3357	Plagioclase	Amphibole	0.295	2.174	1.45289	Sheet silicate				
KRM51/4848	Plagioclase	Augite	0.205	1.591	0.21813	Vermiculite (?)				
KRM51/4850	Plagioclase	Augite	0.230	2.508	4.83768	Closed, chlorite				
KRM51/4850	Augite	Augite	0.030	0.138	0.98684	Chlorite				
KRM51/4852	Augite	Plagioclase	0.105	0.850	1.55281	Sheet silicate				
KRM51/4852	Plagioclase	Plagioclase	0.150	1.618	5.25128	Sheet silicate				
KR5095A/4834	Quartz	Quartz	0.100	0.577	1.01860	Open	321	0.02226	0.02483	0.04709
KR5095A/4836	Quartz	Quartz	0.020	0.213	0.02218	Open				
KR5095A/4839	Quartz	Quartz	0.015	0.147	0.00453	Open				
KR5095A/5839	Quartz	Quartz	0.326	3.187	1.04002	Open				
KR5095A/5840	Quartz	Quartz	0.263	2.508	0.01425	Open				
KR5095A/5841	Quartz	Quartz	0.176	1.650	1.73783	Open				

Note: Mineral types are identified by polarized-light microscopy and TEM EDX analyses. The average grain diameter per sample is based on diameters of opposing grains at measured boundaries or on distances between boundaries and cracks, given in Table S1. The widths of boundaries are taken from TEM images as shortest distance perpendicular to opposing, strictly parallel grain faces, unless an oblique opening direction can be inferred. Due to sharpness of images and the general orthogonality of the boundaries to the image plane, the inaccuracy of measurement is estimated as only 5 nm. Fillings of open grain and phase boundaries and cavities are determined, based on their textures, on semi-quantitative TEM EDX analyses, and diffraction data. The area of dissolved matter is measured directly in the images (Figure 1b) and related to the total length of open or filled boundary in the foil. The determination scheme for Vol-% of open/filled boundaries and dissolution cavities is given in Table S2. nd = not determinable.

southeastern margin of the Joshua Flat Pluton (White-Inyo Mountains, California, USA), roughly 100 m horizontally away from the steep contact, where synmagmatic foliations and lineations are developed (Kruhl & Paterson, 1992; Morgan et al., 1998). At constant pressure of 2.5–3 kbar, the monzonite cooled to sub-greenschist to lowermost greenschist facies temperatures of the wall rocks (Figure 2; Ernst, 1996; Ernst et al., 1993; Kontny & Dietl, 2002; Nabelek & Morgan, 2012). After intrusion and crystallization, the monzonite was only affected by low-grade regional metamorphism (Ernst et al., 1993).

The three analysed quartz–K-feldspar, quartz–amphibole, and plagioclase–amphibole boundaries, with a total length of ~24 μm (Table S1), are a few hundred nanometre wide and partly filled with sheet silicate, biotite, amphibole, and possibly quartz (Table 1; Figure 10 and Figure S2). The quartz–amphibole and quartz–K-feldspar phase boundaries are straight; the faces of the opposing grains are strictly parallel, and dissolution cavities are not visible. In contrast, the plagioclase–amphibole phase boundary appears stepped, with small dissolution cavities (Figure 11). Both crystal faces are locally covered by biotite. The average volume of open/filled boundaries and cavities adds to ~0.94% and ~0.33% (Table 1).

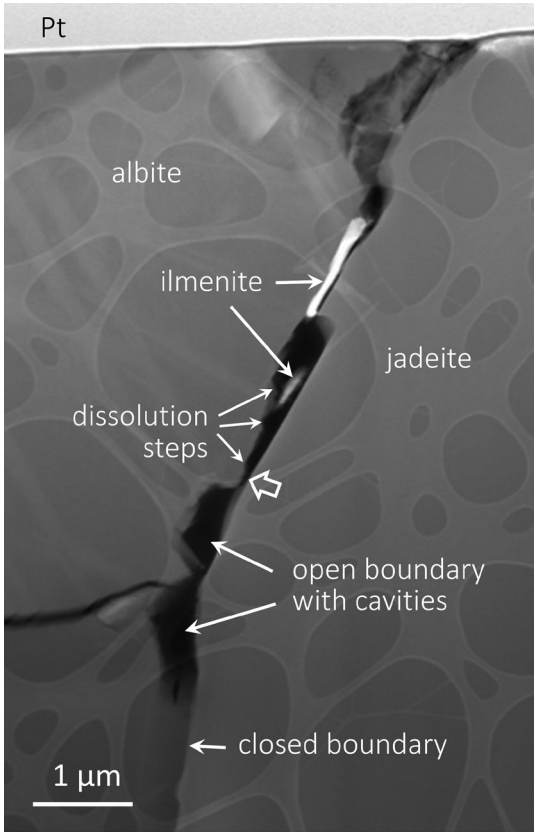

FIGURE 4 HAADF TEM image of a partially open phase boundary between albite and jadeite. Jadeite quartzite from the Shuanghe region, Dabie Shan (Central Eastern China); sample RP11, foil 4840. Light band (Pt) is a protective layer of platinum covering the thin-section surface prior to FIB milling. The initially probably ~50 nm open boundary (short, open arrow) locally forms up to 500 nm wide dissolution cavities with dissolution steps and is partly filled with precipitated Fe–Ti-oxide, probably ilmenite. Dissolution steps reach mostly into the albite. Mineral identification is based on polarized-light microscopy and semi-quantitative TEM EDX analyses

3.6 | Tholeiitic basalt (sample KRM51)

The sample is composed of mostly plagioclase (andesine), clinopyroxene (augite), and olivine (Figure 3e). It comes from the late-Tertiary volcanism in the Hegau (southwest Germany) (Keller, 1984). Phonolite and basalt lava crystallized close to the surface (Schreiner, 1984) and, consequently, rapidly cooled at nearly atmospheric pressure (Figure 2).

Eight grain and phase boundaries between plagioclase, amphibole, and clinopyroxene, with a total length of ~64 μm (Table S1), were analysed. They are open in the range of 30 to ~300 nm (Table 1), locally extend to large cavities, and are nearly totally filled with sheet silicate, partly chlorite (Figure 12a). The sheet-silicate flakes are variably orientated and locally offset with gashes between batches of sheet-silicate layers (Figure 12b). The average volume of filled boundaries and cavities adds to ~0.80% and ~1.36% (Table 1).

3.7 | Hydrothermal quartz (sample KR5095A)

The sample is composed solely of hydrothermal quartz from the central part of the Bavarian Pfahl shear zone (Germany). The Pfahl formed during late Permian to early Triassic (Horn et al., 1986). For its central part, *P–T* conditions of quartz formation of ~210–250°C and ~0.5–1.6 kbar are estimated (Oppermann, 1990; Peucker-Ehrenbrink & Behr, 1993; Schaarschmidt et al., 2019). These temperatures are clearly below the brittle–ductile transition of quartz (Figure 2). Mesoscale fabrics indicate dissolution and precipitation in micrometre to millimetre-grained masses of different quartz generations (Yilmaz et al., 2014).

The six analysed quartz grain boundaries with a total length of ~55 μm (Table S1) are open in the range of 15 to more than 300 nm and do not contain any filling (Table 1). Locally, two neighbouring grains are connected by 'bridges' or 'islands' slightly oblique to the grain faces (Figure 13). Cavities with segmented, crystallographically controlled faces, and dislocations at cavity tips are present (Figure 1b). The average volume of open boundaries and cavities adds to ~0.02% (Table 1).

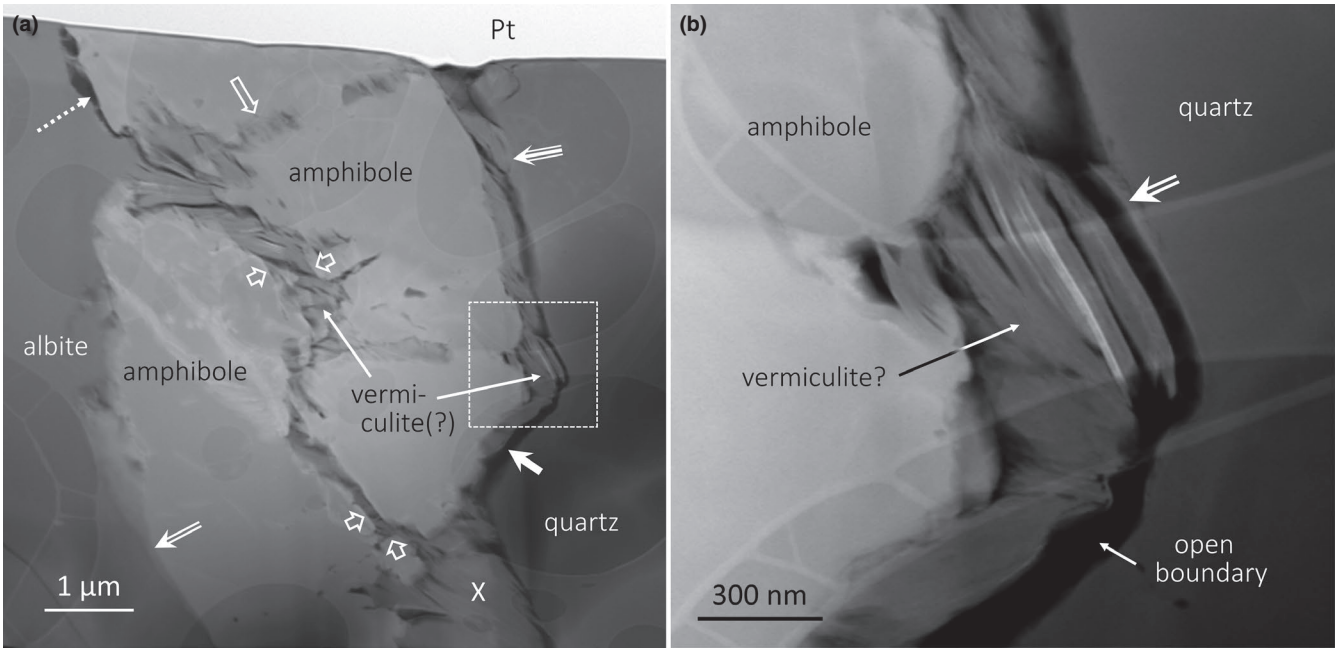

FIGURE 5 HAADF TEM image of partially open and partially filled phase boundaries and fractures from albite–amphibole symplectite between jadeite and quartz. Jadeite quartzite from the Shuanghe region, Dabie Shan (Central Eastern China); sample RP11, foil 4838. (a) The boundary between albite and amphibole is mostly closed (double arrow), except the upper part (broken arrow). A fracture in amphibole and the boundary between amphibole and quartz are filled with a strongly layered mineral, probably vermiculite. Straight, partly parallel boundary segments (short, open arrows) are crystallographically controlled and point to dissolution. Sheet silicate layers perpendicular to a smaller fracture (long open arrow) partly replace the amphibole parallel to cleavage planes. The amphibole–quartz phase boundary is ~250 nm open. Larger dissolution cavities (X) are filled with sheet silicate of variable orientation. Locally, sheet silicate layers are obliquely 'bridging' the amphibole–quartz boundary and are lifted against each other and offset (triple arrow). The boundary between quartz and sheet silicate is partly open (thick, short arrow). Where the quartz–amphibole phase boundary meets the thin-section surface a small depression exists, a result of thin-section preparation and the relatively soft sheet-silicate filling. The light band (Pt) is a protective layer of platinum covering the thin-section surface prior to FIB milling. Mineral identification is based on polarized-light microscopy and TEM EDX analyses. The box indicates the position of (b). (b) Enlarged section of Figure a, with details of the filled quartz–amphibole phase boundary. 10–100 nm thin sheet-silicate layers are offset and lifted against each other. The boundary between sheet silicate and quartz is completely open, except one sheet-silicate layer that is still attached to the quartz (double arrow)

4 | DISCUSSION

First, we will examine the two different types of grain and phase boundary-related porosity—open boundaries and larger cavities—and their formation, and then the compositional and textural variation of the filling. Finally, we discuss the consequences for metamorphic and surface processes.

Except one completely closed boundary, all other boundaries, fractures and the cleavage plane are partly to entirely open in the range of up to several hundred nanometres and partly to totally filled with secondary minerals. In detail, 80 of 92.5 µm total length of the analysed 10 quartz grain boundaries are open; that is 86.5% (Table S1). Adding data of 23 quartz grain boundaries presented in Kruhl et al. (2013, Table 1) leads to 87.5% open boundaries in total, that is, does not change the result. The grain and phase boundaries of plagioclase, K-feldspar, clinopyroxene, amphibole, and calcite; their boundaries with quartz; and cracks and cleavage planes in these minerals (38 in total) show similar values. Before refilling, they are open over ~95% of their total length of ~287 µm (Table S1). Although the data basis is still small and differences between the different samples exist, the percentage of open and refilled boundaries is consistently high. This allows us to conclude that the processes leading to the observed high amount of open and refilled boundaries are widespread and general.

4.1 | Grain and phase boundary-related porosity

Under the TEM most boundaries are straight or only rarely and weakly faceted. Along open sections, the opposite grain faces frequently run exactly parallel (Figures 8a, 10a and Figure S3) even if kinks are present (Figures 1b and 13). This excludes dissolution-driven removal of solid matter and indicates opening of the boundaries by movement of the two

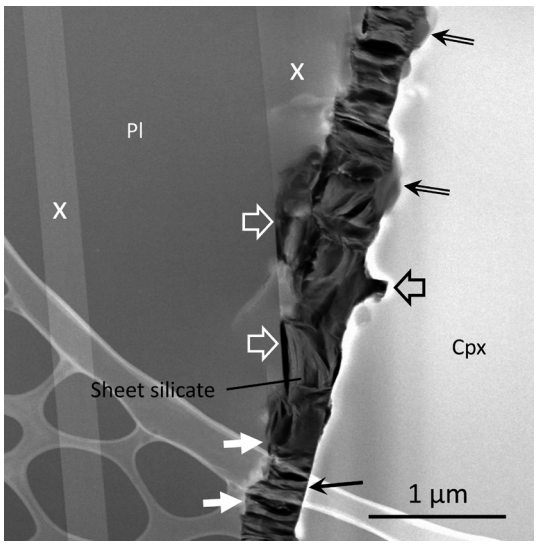

FIGURE 6 HAADF TEM image of a ~350–400 nm thick, filled phase boundary between plagioclase (Pl), with lamellar albite deformation twins (x), and clinopyroxene (Cpx–diopside) from a granulite facies metagabbro of the lowermost exposed part of the fossil Variscan lower continental crust of Calabria (southern Italy). Sample KR3238B, foil 4843. The boundary is filled with sheet silicate of variable orientation—perpendicular, oblique, or parallel to the boundary. Locally, the boundary is straight against pyroxene (black arrow) or forms broad (black double arrows) or slim, deep bulges (black, thick, open arrow). Boundary steps against the plagioclase (white, thick arrows) are partly controlled by a deformation twin boundary (white, thick, open arrows). Mineral identification is based on polarized-light microscopy and TEM EDX analyses

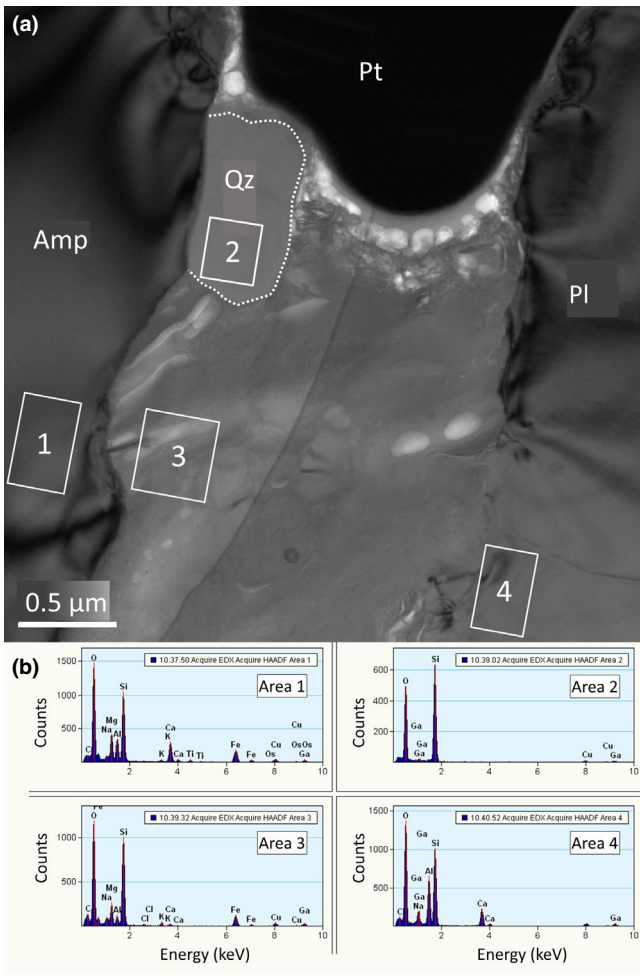

FIGURE 7 (a) HAADF TEM image of a ~1.5 µm thick, filled phase boundary between amphibole (Amp) and plagioclase (bytownite) (Pl) from a granulite facies metagabbro of the lowermost exposed part of the fossil Variscan lower continental crust of Calabria (southern Italy). Sample KR3238B, foil 2880. Platinum (Pt) forms a protective layer covering the thin-section surface prior to FIB milling. It fills the 'eroded' boundary close to the thin-section surface. Subhedral quartz (Qz; dotted outline) is present in the phase boundary, together with sheet-silicate, indicated by semi-quantitative TEM EDX analyses and the flaky structure of the mineral. The variable orientation of layers shows that the sheet silicate did not grow on the expense of the neighbouring amphibole or plagioclase. Mineral identification is based on polarized-light microscopy and TEM EDX analyses. Numbers point to measured areas. (b) Semi-quantitative EDX measurements within the areas outlined in (a)[Colour figure can be viewed at wileyonlinelibrary.com]

grain faces away from each other. However, the true distance and direction of opening can only be inferred in special cases, for example, if opposing kinks of both crystal faces are present (Figure 1b). Consequently, the true translation distance of two opposing crystal faces can exceed but never fall below the widths of open boundaries, given in Table 1. These values extend from 15 to ~600 nm and are in the range recently observed in rocks from contact and regional metamorphism (Kruhl et al., 2013). The percentage of pore space of open and partly filled boundaries varies significantly from one to the other rock type (Table 1). It is by far lowest in hydrothermal quartz masses that formed at ~210 to 250°C (Figure 2), is increased in metamorphic rocks, and reaches values of 0.8 and close to 1% in the two samples of volcanic and plutonic rocks.

To some degree, the present data support the model that opening of grain and phase boundaries is related to anisotropic volume reduction during exhumation (Kruhl et al., 2013). Although the grain diameter measurements can be fraught with large errors, a weak correlation exists between opening width and grain size, that is, the average diameter in 2D of the two neighbouring grains (Figure 14). This correlation is particularly obvious if the hydrothermal quartz and the jadeite quartzite are excluded, which experienced comparatively low temperature or high pressure.

Data from specific rocks provide further arguments for the model. (a) The relatively small opening width in hydrothermal quartz corresponds with the formation of quartz clearly below its brittle–ductile transition (Figure 2). During cooling from such a low temperature to room temperature, the volume of quartz decreases by only ~0.3%, depending on

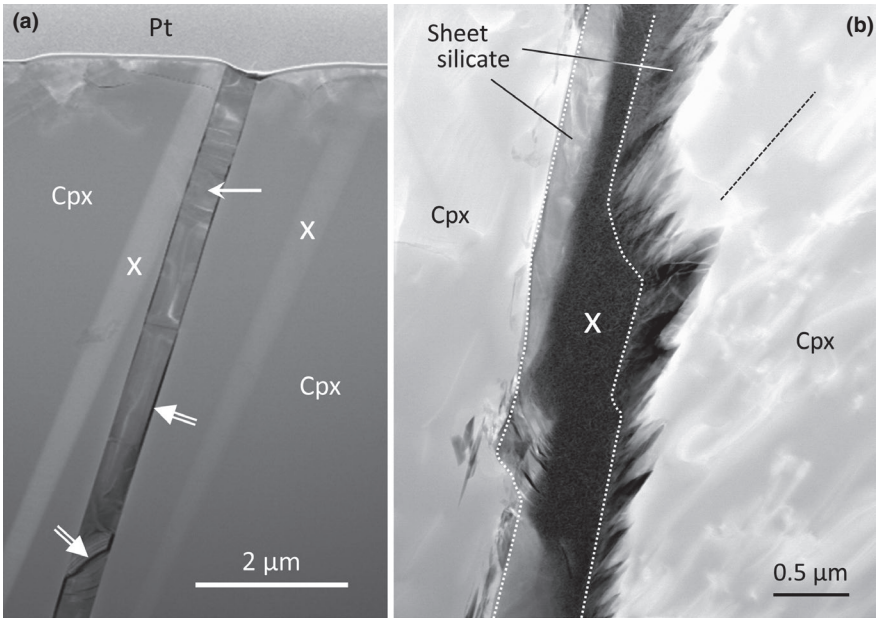

FIGURE 8 HAADF TEM images of fracture and grain boundary from felsic granulite of the lowermost exposed part of the fossil Variscan lower continental crust of Calabria (Southern Italy); sample KR3434B. (a) Nearly 500 nm wide fracture in clinopyroxene (Cpx) filled with sheet silicate (arrow). Up to 50 nm wide, open space (double arrows) between filling and clinopyroxene as well as between sheet silicate layers point to a second stage of opening. Dissolution cavities are not visible. The two parallel, light grey stripes (X) probably represent exsolution lamellae. Thin-section preparation led to a small depression where the fracture meets the thin-section surface. The light grey band (Pt) is a protective layer of platinum covering the thin-section surface prior to FIB milling. Foil 4833. (b) Roughly 500 nm thick, filled boundary between two clinopyroxene grains (Cpx–diopside). The clinopyroxene on the right contains numerous lattice defects (diffuse light bands) well aligned obliquely to the grain boundary (black broken line). The boundary is filled with sheet silicate (probably vermiculite) and amorphous matter (X). The boundaries between sheet silicate and diopside or amorphous matter are straight (white dotted lines) with local steps. On one side of the boundary sheet silicate layers are oriented parallel to the planar arrangement of lattice defects (black broken line) and form replacement textures. Mineral identification is based on polarized-light microscopy and semi-quantitative TEM EDX analyses. Foil 4835

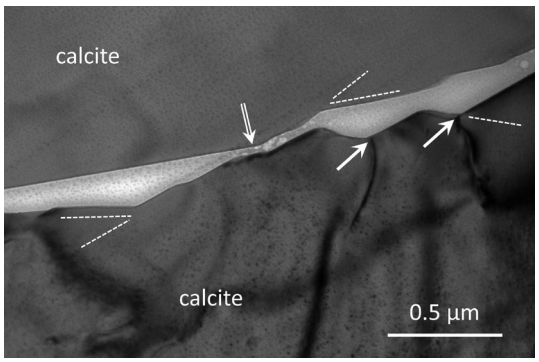

FIGURE 9 HAADF TEM image of two neighbouring calcite grains from pure calcite marble (Alpi Apuane, Carrara, Tuscany/Italy); sample W238, foil 2771. At the thinnest location (double arrow), the grain boundary is ~40 nm open with the two grain faces parallel to each other. Boundary segments occupy three different, crystallographically controlled orientations (broken lines) and form conical cavities where dislocations meet the grain face (arrows)

the decompression-related volume expansion (Kihara, 1990; Levien et al., 1980). The driving force of quartz grain-boundary cracking is weak (Taylor, 1972). Both may contribute to the low opening values (Figure 14). (b) In basalt and monzonite, widths of boundaries are relatively large and ratios between these widths and grain diameters are low. This agrees with the fact that the involved minerals pass their brittle–ductile transitions at relatively low pressure (Figure 2), where decompression-related volume expansion does not markedly work against the cooling-related volume reduction.

However, it must not be ignored that, for example, the values of the jadeite quartzite measurements and their broad scattering do not fit the proposed scheme (Figure 14). This can be seen as indication that more processes behind the boundary opening have to be considered. Moreover, it is definitely a handicap that the measurements as well as the semi-quantitative model are only related to 2D. Recently, first steps have been taken into 3D numerical forward modelling of cooling–decompression paths below 300 MPa and 300°C (Raghami et al., 2020). They show that grain boundaries crack and increasingly widen during cooling and the proportion of open grain boundaries is in the range observed in natural rocks. This argues for the validity of the proposed opening process.

By no means, cracking of boundaries is related to tectonic stress. Brittle deformation structures are not observed

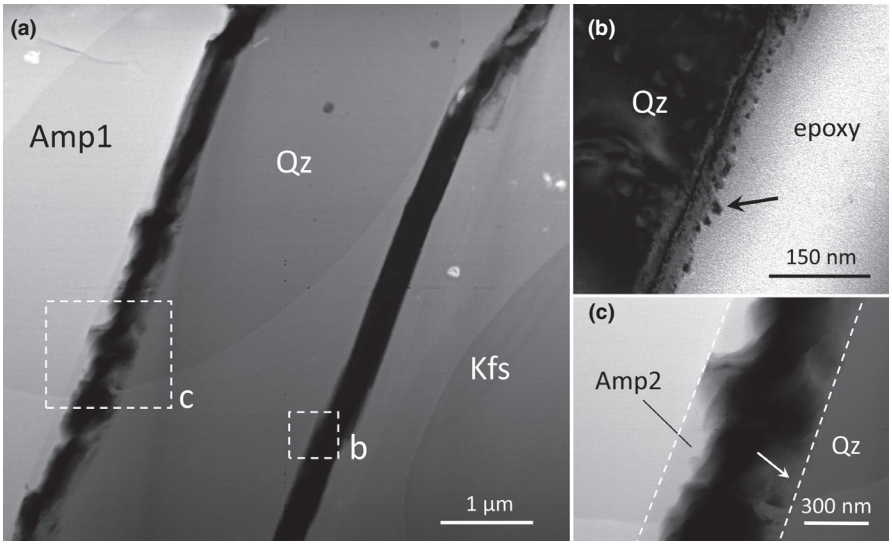

FIGURE 10 HAADF TEM image of phase boundaries between amphibole (Amp1), quartz (Qz), and K-feldspar (Kfs) from amphibole monzonite (Joshua Flat Pluton, White-Inyo Mountains, California); sample KR3720, foil 2881. (a) The boundaries are straight, only weakly facetted, open up to ~600 and 350 nm, and party filled with secondary phases. The boxes mark the positions of the enlarged sections b and c. (b) The boundary between quartz and K-feldspar is nearly completely open, that is, filled with epoxy. A film of euhedral crystals, possibly quartz (black arrow), covers the face of the quartz grain. (c) The boundary between amphibole and quartz is partly filled. The face of the amphibole grain is covered by an irregular mass of amphibole with slightly increased Mg and decreased Al content (Amp2). The face of the quartz grain is covered by an irregular mass of sheet silicate, possibly biotite (white arrow). The white broken lines mark the two parallel grain faces. Mineral identification is based on semi-quantitative TEM EDX analyses

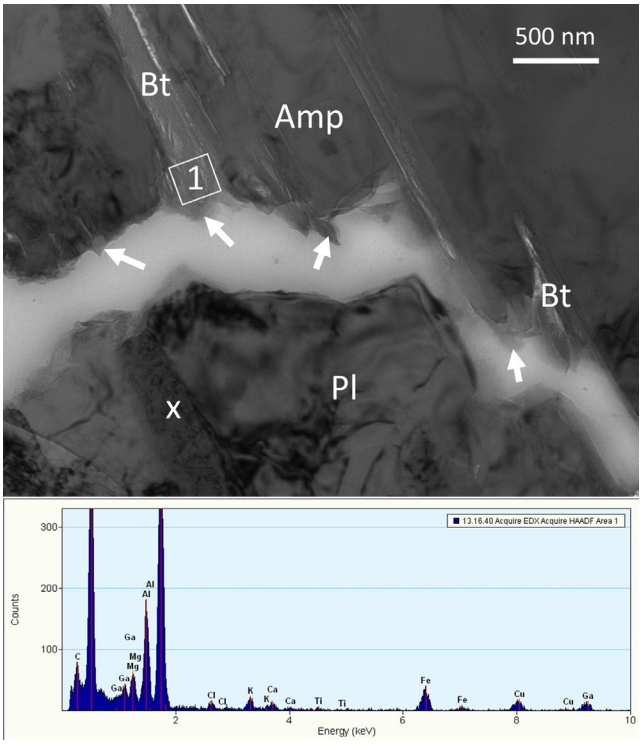

FIGURE 11 HAADF TEM image and semi-quantitative TEM EDX analysis of amphibole (Amp) and plagioclase (Oligoclase) (Pl) and their partly filled phase boundary. Biotite (Bt) replaces amphibole along cleavage planes and partly covers the two grain faces along the open boundary (arrows). EDX analysis from area 1; x = lamellar twin in plagioclase; amphibole monzonite from the Joshua Flat Pluton (White-Inyo Mountains, CA); sample KR3720, foil 2876[Colour figure can be viewed at wileyonlinelibrary.com]

on grain scale except isolated microfractures within grains of garnet, clinopyroxene, and amphibole (Figure 3a–c). In all TEM images, along open boundaries the crystal faces of opposing grains do not show any signs of brittle deformation.

4.2 | Cavities

In all samples a certain number of open boundaries locally widen to nanometre to few micrometre-sized cavities, which typically extends into the adjoining grains with straight, crystallographically controlled facets, mostly where dislocations meet grain faces (Figures 1b, 4, 8 and 9). They resemble dissolution pits described from mid-crustal quartzofeldspathic ultramylonites (Billia et al., 2013; Mancktelow & Pennacchioni, 2004). In addition, the connectivity of open boundaries and cavities in 3D, which allows pervasive fluid flow, is also demonstrated by FIB-SEM tomography (Video S1). The video of the 3D development of three grain boundaries in Carrara marble documents how the locations of open boundaries and related cavities change in 3D and how the boundaries open and close even on the nanometre scale. The video displays the enormous variability of grain boundary and cavity structure and position in 3D. These observations strongly argue for dissolution and probably also precipitation during fluid flow in a network of partially open grain and phase boundaries.

The area of cavities measured in TEM foils (Figure 1b; Kruhl et al., 2013, Figure 4a), equivalent to the volume of

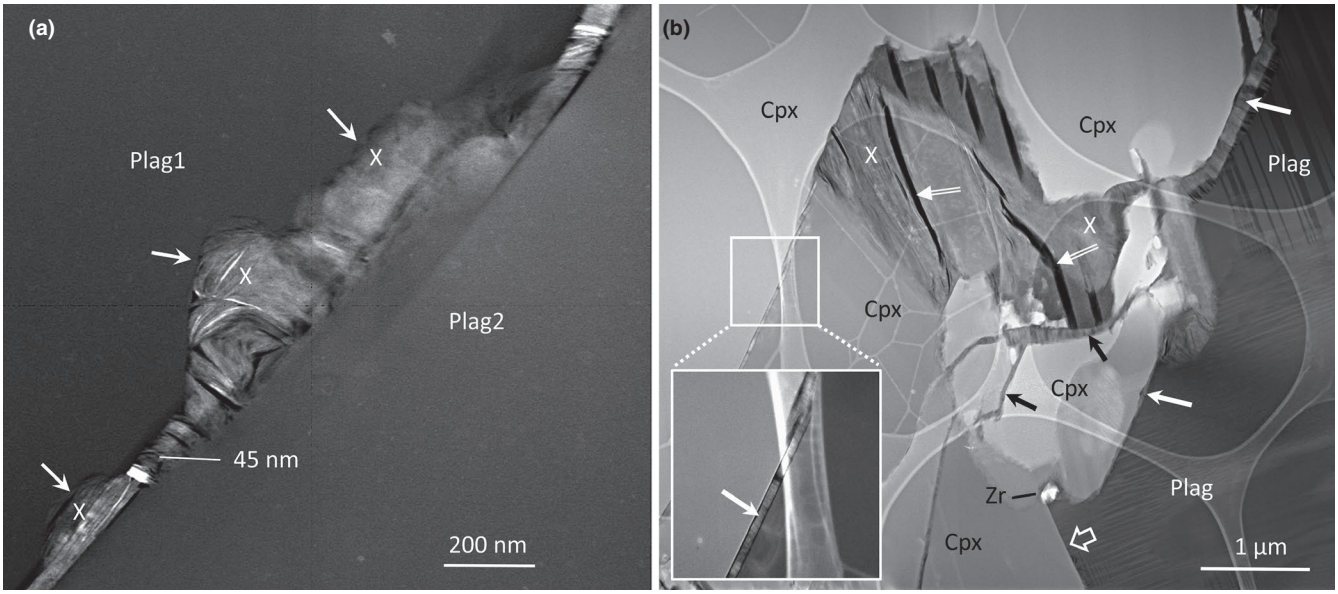

FIGURE 12 HAADF TEM images of boundaries between plagioclase and clinopyroxene grains of tholeiitic basalt from late-Tertiary volcanism in southwest Germany (Hegau). Sample KRM51, foils 3347 and 4850. (a) Straight, ~45 nm open boundary between two plagioclase grains (Pl1 and Pl2) and large cavities (X) completely filled with sheet silicate, partly chlorite. The cavities border upon the plagioclase grains with straight segments (arrows). Variable orientation of sheet silicate layers and straight faces of the grain boundary indicates that sheet silicate does not replace plagioclase but fills an initially open grain boundary. (b) Phase boundaries between plagioclase (Pl) and clinopyroxene (Cpx) are locally closed (short, open arrow) but mostly filled with sheet silicate (white arrows). Sheet silicate also fills a large cavity (X), fractures in clinopyroxene, and the boundary between clinopyroxene and the sheet silicate filling of the cavity (black arrows). The offset of sheet silicate layers and lift against each other form open space (white double arrows). A nanometre-sized zircon crystal (Zrn) pins the clinopyroxene–plagioclase boundary. Mineral identification is based on polarized-light microscopy and semi-quantitative TEM EDX analyses

dissolved matter, is different in different rocks (Table 1). It is by far highest in basalt, with ~1.36 vol.%, and lowest in jadeite quartzite and hydrothermal quartz, ranging from ~0.07 to ~0.025 vol.%. The intense dissolution in basalt is probably due to flow of hot fluids during cooling. Vice versa, this can be taken as argument for opening of the grain and phase boundaries and generation of a connected pore space not too long after crystallization of the basalt. The relatively high value of dissolution in marble probably results from the high solubility of calcite with decreasing temperature (Segnit et al., 1962).

It should be noted that the cavities are solely connected with open boundaries. Together, both form porosity clearly developed below conditions of peak metamorphism or crystallization. Our observations, however, limited to the nanometre scale, do not point to any porosity formed at high *P–T* conditions.

4.3 | Filling of grain and phase boundaries and cavities

Most of the 43 open grain and phase boundaries, four fractures and one cleavage plane, are partly or totally filled with secondary minerals (Table 1), mainly sheet silicate. However, a few fillings are composed of euhedral quartz, ilmenite, biotite, felted masses of amphibole, and amorphous matter. Sheet silicate fills open boundaries and cavities with variable orientation, mostly oblique to grain faces and with different orientations in different parts of the filled boundary (Figures 5a, b, 6 and 12a,b) and only rarely grows into the adjoining grains parallel to cleavage planes (Figure 5a) or to planes of planar lattice defects (Figure 8b). From these observations, it follows that initially grain and phase boundaries, fractures and cleavage planes opened, cavities were leached out of the neighbouring grains, and subsequently pore space was filled with matter precipitated from fluids.

The mineralogy of fillings roughly corresponds to the mineralogy of the rocks. Chlorite, albite, and possibly actinolite occur in metagabbro and basalt; amphibole and biotite in amphibole monzonite; ilmenite and sheet silicate in jadeite quartzite; and sheet silicate in Cpx-granulite and in the rocks mentioned beforehand (Table 1). Quartz and calcite grain boundaries do not contain fillings except possibly precipitated quartz and calcite. Consequently, fluid-based transport of matter did not occur over larger distances but the material originates from the respective rocks or even from the microscale environment, as known for long from observations

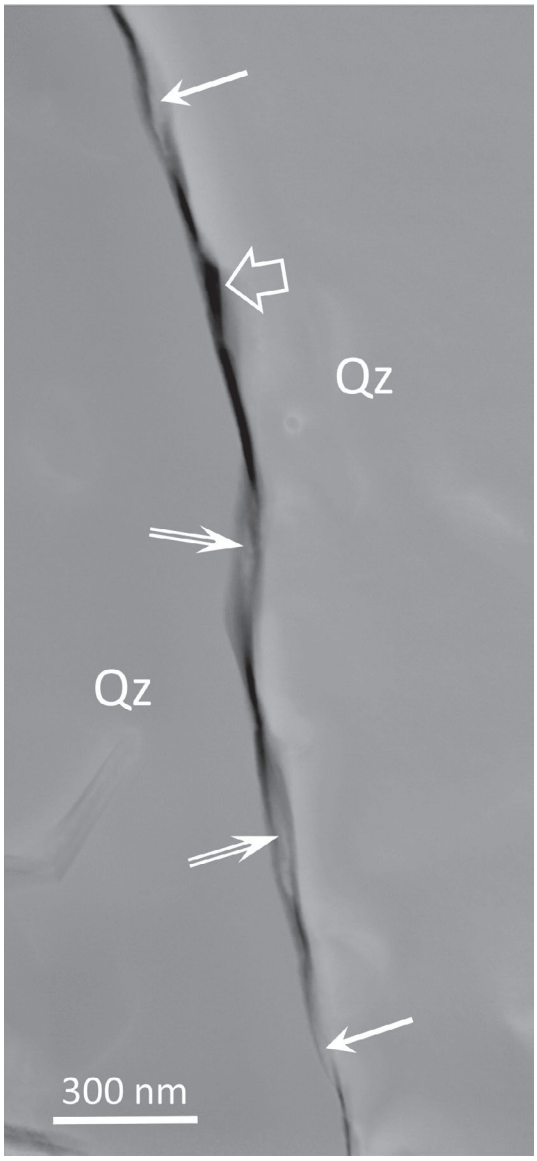

FIGURE 13 HAADF TEM image of hydrothermal quartz from the Bavarian Pfahl shear zone (Germany). Sample KR5095A, foil 4834. A relatively straight and ~20 nm open boundary separates two quartz grains (Qz). Locally, the grains are connected by 'bridges' (arrows) or 'islands' (double arrows). Indications of week dissolution are rare (short, open arrow)

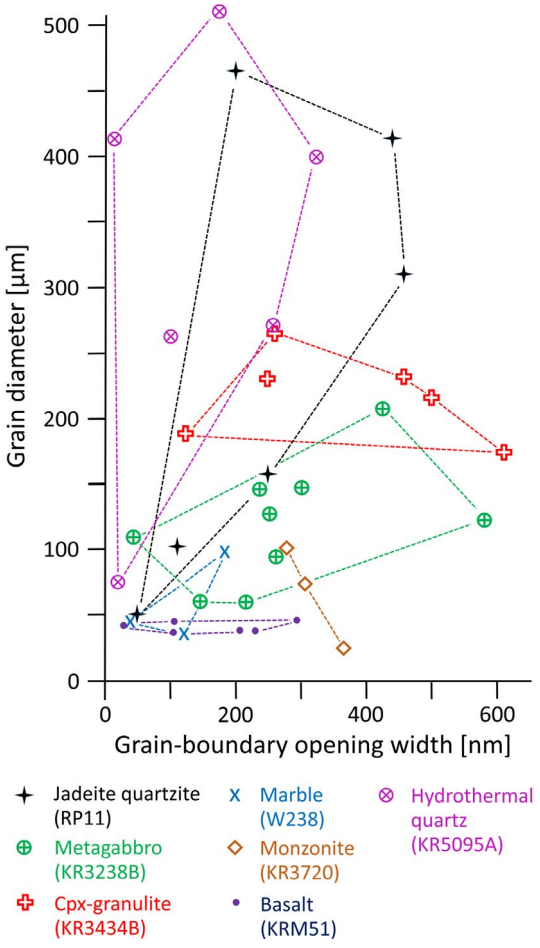

FIGURE 14 Correlation between width of open grain and phase boundaries and average diameter of the two opposing grains. Determination of diameters and opening width described in Table 1. Broken lines outline the distribution of measurement points of the same sample [Colour figure can be viewed at wileyonlinelibrary.com]

of foliation-parallel quartz and calcite veins in metamorphic rocks (Voll, 1960, 1969).

Amorphous matter in grain boundaries of clinopyroxene (Figure 8b) is enriched in Al, K, and C and depleted in Ca, compared to clinopyroxene (Figure S4) and most probably represents silica gel. The geometrically fitting opposing steps of the boundary between sheet silicate and amorphous matter (Figure 8b) indicate formation of the latter during a late stage of filling or after a second stage of grain-boundary opening. Konrad-Schmolke et al. (2018) report similar alkali-Al–Si-rich amorphous matter in pore space between amphibole crystals in high-*P*/low-*T* rocks and interpret this as the result of polymerization of the crystal lattices. These authors suggest that amorphous matter plays an important role in dissolution–precipitation processes. It is an open question if such a role can be also assumed for the studied samples.

Sheet-silicate layers are not only variably oriented in different parts of open boundaries and cavities but locally also clinched and bent (Figures 6 and 12) or offset and lifted against each other or against the opposing grain faces (Figure 5). These observations point to nucleation and growth during different stages of opening and indicate that filling occurred contemporaneously as well as subsequently to dissolution during the probably long-lasting period of cracking and widening of grain and phase boundaries. Specifically, the offset and lift of sheet-silicate layers (Figure 12b) argue for a second stage of opening and/or for displacement of neighbouring grains relatively to each other. Oblique 'bridges' between neighbouring grains, resembling en-echelon structures (Figure 13), also indicate such displacement. This probably results from rearrangement of the grain aggregate

due to different elastic response of grains to cooling and decompression.

Thirteen boundaries do not contain any filling: three quartz grain boundaries and one albite grain boundary from the UHP jadeite quartzite, six grain boundaries from hydrothermal quartz mass, and three calcite grain boundaries from marble. It can be only speculated if the lack of filling results from (a) the absence of fluids with sufficient amount of dissolved matter, (b) the difficulty to recognize precipitated matter equalling the host mineral, or (c) conditions unsuitable for precipitation of matter. At least for the UHP quartzite, the absence of fluids with dissolved matter can be excluded because boundaries contain vermiculite and ilmenite within micrometre- to millimetre distance to unfilled boundaries.

4.4 | At which temperature do boundaries open?

Based on grain-boundary opening measurements in quartzite, Kruhl et al. (2013) suggest that boundaries open below the brittle–ductile transition of the involved minerals. However, the currently available data on boundary fillings do not clearly support this model. The secondary minerals are mostly chlorite, vermiculate, and other sheet silicates, and rarely biotite and actinolite (Table 1). They represent products of lowermost metamorphism. Only biotite and actinolite indicate greenschist facies conditions, however, not necessarily exceeding lowermost greenschist facies (Bucher & Frey, 2002). Two reasons for lack of higher temperature fillings can be quoted. First, with 48 boundaries, cracks, and cleavage planes the number of measurements is still low and additional measurements from boundaries in different rocks might reveal higher temperature fillings. Second, although the cooling-related volume reduction may become effective below the brittle–ductile transition, cracking of boundaries also depends on their tensile yield strength. Three-dimensional grain scale numerical modelling suggests that grain-boundary opening in quartz initiates ~80°C below the brittle–ductile transition, that is, at roughly 220°C (Raghami et al., 2020). It can be assumed that the proportion of open grain boundaries, sufficient for permeability, and formation of secondary minerals from fluids, is reached at even lower temperatures. This probably also holds for other minerals because the underlying processes of thermoelastic behaviour are generally valid.

4.5 | Effects on metamorphic and surface processes

Although the studied samples do not show retrograde alteration on the specimen or micro-scale, alteration on the nanometre scale is visible in some cases (Figures 5a and 8b). This shows that the network of connected, entirely or partly open grain and phase boundaries not only serves as pathway for fluid flow but also triggers reactions during retrograde conditions of at least lower greenschist facies, that is, at depths down to lowermost parts of the upper crust. The increased dissolution at dislocation cores (Figures 1b and 9), together with mineral replacement at these sites (Figure 8b), highlights the importance of dislocations and of dislocation-generating deformation for metamorphic reactions. This is in agreement with the view that stress distribution on the grain scale can control the initiation of metamorphic reactions (Wilson et al., 2009).

Specifically, the analysed basalt sample (KRM51) shows high porosity. Even though the porosity related to open boundaries only slightly exceeds that of other rocks (Table 1), the dissolution-related porosity is more than four times higher compared to marble (W238) and monzonite (KR3720) and 10–50 times higher than in the other rocks. Sheet silicate and chlorite nearly totally fill open boundaries and cavities as well as cracks between the filling and faces of neighbouring crystals (Figure 12). This can be considered as the result of intensive dissolution and precipitation during the cooling period of the basalt, which should be in the range of several years, that is, a geologically short period (Peck et al., 1977).

A large number of metamorphic reactions are triggered and kept active by fluids (Yardley, 1989). Consequently, permeability on grain scale is a crucial parameter in metamorphism. This is especially true for retrograde reactions. Retrograde metamorphism often occurs along zones of intensified deformation and such high-strain zones are seen as structures that can strongly channelize fluid flow (Vernon, 2004, Chapters 4.13.2 and 5.6.5). In addition, networks of partially open grain and phase boundaries, together with dissolution cavities, could represent grain-scale precursors of these visible fluid pathways.

Particularly, metasomatism needs pervasive fluid access. This requires permeability on the grain scale, caused by, for example, deformation-induced grain-scale dilatancy, hydraulic fracturing, or mineral replacement reactions (Putnis & Austrheim, 2013). In addition, networks of open grain and phase boundaries may strongly contribute to permeability and, consequently, to fluid flow during metasomatism. This is also supported by the observation that metasomatism often occurs during late stages of uplift and cooling in high-grade metamorphic regions (Yardley, 2013). Under such conditions, networks of partially open grain and phase boundaries are present.

It can be speculated, in which way and how strongly partially open boundaries contribute to fluid flow and reactivity in rocks during polymetamorphism. Our investigations show that grain and phase boundaries in metamorphic or magmatic rocks, crystallized at depth and subsequently exhumed,

typically open and are filled with secondary minerals. With rare exceptions, these fillings do not form from the surrounding grains but from the fluid in the pore space. It follows that many, if not the vast majority of igneous and metamorphic rocks, contain secondary minerals even if they appear totally unaltered and 'clean', not only in hand specimen but also on microscale, that is, under the polarized-light microscope.

These fillings form a fluid reservoir even in nominally dry rocks. They may serve as nuclei of new metamorphic minerals during increasing temperature, that is, trigger metamorphic reactions, and contribute to the development of rocks during prograde metamorphism. Moreover, such fillings may strongly enhance deformation by grain-boundary glide as well as pressure solution under low-grade metamorphic conditions and reduce the strength of rocks in deformation experiments.

One of the most significant contributions of partially open grain and phase boundaries is related to weathering. Here, we do not consider weathering under extreme temperature variation well known from arid conditions (Skinner & Porter, 1989) leading to rock disintegration on large scale, but weathering under 'normal' surface conditions. Under such conditions, the network of partially open boundaries allows gases and liquids to deeply penetrate the rock. This effect is specifically strong where open boundaries are not or only incompletely filled with secondary minerals. Micro-scale mineral alteration textures from various weakly to strongly weathered rocks often show roughly up to 20 μm wide, evenly open cracks along grain and phase boundaries, which are filled with secondary products without affecting the neighbouring grains; denticulation is only locally visible (Delvigne, 1998, Figures 054, 068, 080, 215). It indicates that secondary products mostly did not replace the grain margins of 'closed' boundaries, but filled fissures open prior to weathering. This argues for open boundaries as one pre-condition of weathering.

Not least, partially open boundaries may be important with respect to repositories of nuclear waste. Disposal in deep geological repositories is the preferred option for management of long lived or high-level radioactive waste. Suitable conditions can be found in various types of crystalline, volcanic and argillaceous rocks, as well as in rock salts (IAEA, 2003). For safety of geological disposal, permeability of the bedrock is one of the critical parameters. In a radioactive waste repository various processes can lead to significant amounts of gas, which may migrate through the bedrock (IAEA, 2001). While previous investigations focused on channel and fracture networks as pathways for such gases (Johansson et al., 1998; Neretnieks, 2017), our study shows that grain and phase boundaries, open on the nanometre scale, generate permeability that may affect the migration of released radionuclides through crystalline bedrock. If, however, grain and phase boundaries are filled with secondary minerals the absorptive capacity and, consequently, the bedrock's retention capability for radionuclides is possibly increased. This argues for detailed nanometre-scale studies on grain and phase boundaries in potential bedrocks of underground disposals of radioactive waste.

5 | CONCLUSIONS

Based on FIB sample preparation, TEM and 3D slice and view imaging (FIB/SEM) show that, in a variety of metamorphic, plutonic, volcanic, and hydrothermal rocks, open and partially refilled grain and phase boundaries as well as connected cavities occur on the scale of several hundred nanometres to few micrometres.

(i) Such pore space appears to be a common phenomenon in most if not all types of crystalline rock. It is definitely not related to sample or thin-section preparation and does not represent FIB-induced artefacts. Arguments have been presented in detail by Kruhl et al. (2013).

(ii) Most probably, cracking and opening of grain and phase boundaries are related to anisotropic thermoelastic response of crystals to cooling. Opening starts clearly below the brittle–ductile transition of the involved minerals. Cavities form subsequently to cracking and opening of boundaries and indicate dissolution and precipitation.

(iii) In the studied samples pore space reaches ~0.05 vol.% in hydrothermal quartz, ~0.2–0.7 vol.% in metamorphic rocks, ~1.26 vol.% in the plutonic rock and nearly 2.2 vol.% in basalt. It forms a network, providing permeability at conditions of at least lowermost greenschist facies.

(iv) Fluid flow through such a network can lead to partial or total filling with secondary minerals, such as biotite, actinolite, quartz, chlorite, vermiculite, and sheet silicates. These fillings affect chemical analyses of rocks that appear totally fresh, not only on specimen scale but also under the polarized-light microscope.

(v) Under low-grade metamorphic conditions and in the general absence of crystal-plastic deformation, specifically sheet-silicate fillings of grain and phase boundaries can enhance deformation by pressure solution and grain-boundary glide.

(vi) Together with dissolution cavities, networks of partially open grain and phase boundaries are potential grain-scale precursors of larger-scale fluid pathways. Possibly, they govern the channelization of fluids leading to zones of retrograde metamorphism and support pervasive fluid access as prerequisite of metasomatism. Under surface conditions, they allow gases and liquids to deeply penetrate rocks and, therefore, represent at least one precondition of weathering.

(vii) Permeability provided by partially open grain and phase boundaries potentially affect the migration of released radionuclides through crystalline bedrock of deep geological repositories of nuclear waste or, if boundaries are filled with secondary minerals, possibly increases the absorptive capacity and, consequently, the bedrock's retention capability for radionuclides.

ACKNOWLEDGEMENTS

Financial support was given by the German Research Foundation (DFG) under grant KR691/36-1 / SCHM390/17-1. We gratefully acknowledge the comments by Bruce Yardley, Bernardo Cesare, and two anonymous reviewers, which greatly helped to improve the manuscript.

DATA AVAILABILITY STATEMENT

The data that support the findings of this study are partly available from the corresponding author upon reasonable request and partly in the supplementary material of this article.

ORCID


Jörn H. Kruhl https://orcid.org/0000-0002-9681-1080

REFERENCES

Altenberger, U., Hamm, N., & Kruhl, J. H. (1987). Movements and metamorphism north of the Insubric Line between Val Loana and Val d'Ossola, N.Italy. *Jahrbuch Geologische Bundesanstalt Wien*, *130*(4), 365–374.

Ayers, J. C., Dunkle, S., Gao, S., & Miller, C. F. (2002). Constraints on timing of peak and retrograde metamorphism in the Dabie Shan ultrahigh-pressure metamorphic belt, east-central China, using U-Th-Pb dating of zircon and monazite. *Chemical Geology*, *186*(3–4), 315–331. https://doi.org/10.1016/S0009-2541(02)00008-6

Beinlich, A., John, T., Vrijmoed, J. C., Tominaga, M., Magna, T., & Podladchikov, Y. Y. (2020). Instantaneous rock transformations in the deep crust driven by reactive fluid flow. *Nature Geoscience*, *13*, 307–311. https://doi.org/10.1038/s41561-020-0554-9

Billia, M. A., Timms, N. E., Toy, V. G., Hart, R. D., & Prior, D. J. (2013). Grain boundary dissolution porosity in quartzofeldspathic ultramylonites: Implications for permeability enhancement and weakening of mid-crustal shear zones. *Journal of Structural Geology*, *53*, 2–14. https://doi.org/10.1016/j.jsg.2013.05.004

Bohlen, S. R., Montana, A., & Kerrick, D. M. (1991). Precise determinations of the equilibria kyanite - sillimanite and kyanite - andalusite and a revised triple point for Al_2SiO_5 polymorphs. *American Mineralogist*, *76*(3–4), 677–680.

Bucher, K., & Frey, M. (2002). *Petrogenesis of metamorphic rocks* (7th ed.). Springer, 341 pp.

Burkhard, M. (1993). Calcite twins, their geometry, appearance and significance as stress-strain markers and indicators of tectonic regime: A review. *Journal of Structural Geology*, *15*(3–5), 351–368. https://doi.org/10.1016/0191-8141(93)90132-T

Cox, S. F. (2007). Structural and isotopic constraints on fluid flow regimes and fluid pathways during upper crustal deformation: An example from the Taemas area of the Lachlan Orogen, SE Australia. *Journal of Geophysical Research*, *112*, B08208. https://doi.org/10.1029/2006JB004734

Delvigne, J. E. (1998). *Atlas of micromorphology of mineral alteration and weathering*. *The Canadian Mineralogist*, Special Publication 3. Mineralogical Association of Canada, 494 pp.

Ernst, W. G. (1996). Petrochemical study of regional/contact metamorphism in metaclastic strata of the central White-Inyo Range, eastern California. *Geological Society of America Bulletin*, *108*(12), 1528–1548. https://doi.org/10.1130/0016-7606(1996)108<1528:PSORCM>2.3.CO;2

Ernst, W. G., Nelson, C. A., & Hall, C. A. (1993). Geology and metamorphic mineral assemblages of Precambrian and Cambrian rocks of the central White-Inyo Range, eastern California. California Department of Conservation, Division of Mines and Geology, Map Sheet 46.

Etheridge, M. A., Wall, V. J., & Vernon, R. H. (1983). The role of the fluid phase during regional metamorphism and deformation. *Journal of Metamorphic Geology*, *1*(3), 205–226. https://doi.org/10.1111/j.1525-1314.1983.tb00272.x

Franceschelli, M., Memmi, I., Carcangiu, G., & Gianelli, G. (1997). Prograde and retrograde chloritoid zoning in low temperature metamorphism, Alpi Apuane, Italy. *Schweizerische Mineralogische und Petrographische Mitteilungen*, *77*, 41–50.

Gross, A. F. K., & Van Heege, J. P. T. (1973). The high-low quartz transition up to 10 kb pressure. *Journal of Geology*, *81*, 717–724.

Hay, R. S., & Evans, B. (1988). Intergranular distribution of pore fluid and the nature of high-angle grain boundaries in limestone and marble. *Journal of Geophysical Research*, *93*(B8), 8959–8974. https://doi.org/10.1029/JB093iB08p08959

Heinemann, S., Wirth, R., & Dresen, G. (2001). Synthesis of feldspar bicrystals by direct bonding. *Physics and Chemistry of Minerals*, *28*(10), 685–692. https://doi.org/10.1007/s002690000142

Heinemann, S., Wirth, R., Gottschalk, M., & Dresen, G. (2005). Synthetic [100] tilt grain boundaries in forsterite: 9.9 to 21.5°. *Physics and Chemistry of Minerals*, *32*(4), 229–240. https://doi.org/10.1007/s00269-005-0448-9

Horn, P., Köhler, H., & Müller-Sohnius, D. (1986). Rb-Sr-Isotopengeochemie hydrothermaler Quarze des Bayerischen Pfahles und eines Flussspat-Schwerspat-Ganges von Nabburg-Wölsendorf/Bundesrepublik Deutschland. *Chemical Geology*, *58*, 259–272.

Huang, W. L., & Wyllie, P. J. (1981). Phase relationship of S-type granite with H_2O to 35 kbar: Muscovite granite from Harney Peak, South Dakota. *Journal of Geophysical Research*, *86*(B11), 1015–1029.

IAEA International Atomic Energy Agency. (2001). The use of scientific and technical results from underground research laboratory investigations for the geological disposal of radioactive waste. *Technical Reports Series*, *1243*, 70 pp.

IAEA International Atomic Energy Agency. (2003). Scientific and technical basis for the geological disposal of radioactive wastes. *Technical Reports Series*, *413*, 80.

Jamtveit, B., Malthe-Sørenssen, A., & Kostenko, O. (2008). Reaction enhanced permeability during retrogressive metamorphism. *Earth and Planetary Science Letters*, *267*, 620–627. https://doi.org/10.1016/j.epsl.2007.12.016

Johansson, H., Siitari-Kauppi, M., Skalberg, M., & Tullborg, E. L. (1998). Diffusion pathways in crystalline rock – Examples from Äspö-diorite and fine-grained granite. *Journal of Contaminant Hydrology*, *35*(1–3), 41–53. https://doi.org/10.1016/S0169-7722(98)00114-4

John, T., Gussone, N., Podladchikov, Y. Y., Bebout, G. E., Dohmen, R., Halama, R., Klemd, R., Magna, T., & Seitz, H.-M. (2012). Volcanic arcs fed by rapid pulsed fluid flow through subducting slabs. *Nature Geoscience*, *5*(7), 489–492. https://doi.org/10.1038/NGEO1482

Keller, J. (1984). Der jungtertiäre Vulkanismus Südwestdeutschlands: Exkursionen im Kaiserstuhl und Hegau. *Fortschritte der Mineralogie Beihefte*, *2*(62), 2–35.

Kerrick, D. M. (1968). Experiments on the upper stability limit of pyrophyllite at 1.8 kilobars and 3.9 kilobars water pressure. *American Journal of Science*, *266*(3), 204–214. https://doi.org/10.2475/ajs.266.3.204

Kihara, K. (1990). An X-ray study of the temperature dependence of the quartz structure. *European Journal of Mineralogy*, *2*(1), 63–77. https://doi.org/10.1127/ejm/2/1/0063

Kligfield, R., Hunziker, J., Dallmeyer, R. D., & Schamel, S. (1986). Dating of deformation phases using K-Ar and $^{40}Ar/^{39}Ar$ techniques: Results from the Northern Apennines. *Journal of Structural Geology*, *8*(7), 781–798. https://doi.org/10.1016/0191-8141(86)90025-8

Konrad-Schmolke, M., Halama, R., Wirth, R., Thomen, A., Klitscher, N., Morales, L. F. G., Schreiber, A., & Wilke, F. D. H. (2018). Mineral dissolution and reprecipitation mediated by an amorphous phase. *Nature Communications*, *9*, 1637. https://doi.org/10.1038/s41467-018-03944-7

Kontny, A., & Dietl, C. (2002). Relationships between contact metamorphism and magnetite formation and destruction in a pluton's aureole, White-Inyo Range, eastern California. *Geological Society of America Bulletin*, *114*(11), 1438–1451. https://doi.org/10.1130/0016-7606(2002)114<1438:RBCMAM>2.0.CO;2

Kruhl, J. H. (1993). The P-T-d development at the basement-cover boundary in the north-eastern Tauern Window (Eastern Alps): Alpine continental collision. *Journal of Metamorphic Geology*, *11*(1), 31–47. https://doi.org/10.1111/j.1525-1314.1993.tb00129.x

Kruhl, J. H., & Paterson, S. R. (1992). Deformation and pluton emplacement; an example from the White-Inyo Mountains (east-central California). Geological Society of America, Cordilleran Section, 88th annual meeting, Book of Abstracts.

Kruhl, J. H., Wirth, R., & Morales, L. F. G. (2013). Quartz grain boundaries as fluid pathways in metamorphic rocks. *Journal of Geophysical Research Solid Earth*, *118*(5), 1–11. https://doi.org/10.1002/jgrb.50099

Lee, V. W., Mackwell, S. J., & Brantley, S. L. (1991). The effect of fluid chemistry on wetting textures in novaculite. *Journal of Geophysical Research*, *96*(B6), 10023–10037. https://doi.org/10.1029/91JB00604

Levien, L., Prewitt, C. T., & Weidner, D. J. (1980). Structure and elastic properties of quartz at pressure. *American Mineralogist*, *65*(9–10), 920–930.

Liou, J. G., Zhang, R. Y., & Jahn, B.-M. (1997). Petrology, geochemistry and isotope data on a ultrahigh-pressure jadeite quartzite from Shuanghe, Dabie Mountains, East-central China. *Lithos*, *41*(1–3), 59–78. https://doi.org/10.1016/S0024-4937(97)82005-1

Mancktelow, N. S., Grujic, D., & Johnson, E. L. (1998). An SEM study of porosity and grain boundary microstructure in quartz mylonites, Simplon Fault Zone, Central Alps. *Contributions to Mineralogy and Petrology*, *131*(1), 71–85. https://doi.org/10.1007/s004100050379

Mancktelow, N. S., & Pennacchioni, G. (2004). The influence of grain boundary fluids on the microstructure of quartz-feldspar mylonites. *Journal of Structural Geology*, *26*(1), 47–69. https://doi.org/10.1016/S0191-8141(03)00081-6

Marquardt, K., Petrishcheva, E., Abart, R., Gardés, E., Wirth, R., Dohmen, R., Becker, H.-W., & Heinrich, W. (2010). Volume diffusion of Ytterbium in YAG: Thin-film experiments and combined TEM-RBS analysis. *Physics and Chemistry of Minerals*, *37*(10), 731–750. https://doi.org/10.1007/s00269-010-0373-4

Morgan, S. S., Law, R. D., & de Saint Blanquat, M. (1998). Aureole deformation associated with inflation of the concordant Eureka Valley-Joshua Flat-Beer Creek composite pluton, central White-Inyo Range, eastern California, Guidebook to field trip #5. GSA annual meeting, Cordilleran Section, Cal. State Univ. Long Beach, Dept. Geol. Sci., 5/1-5/30.

Nabelek, P. I., & Morgan, S. S. (2012). Metamorphism and fluid flow in the contact aureole of the Eureka Valley-Joshua Flat-Beer Creek pluton, California. *Geological Society of America Bulletin*, *124*(1–2), 228–239. https://doi.org/10.1130/B30425.1

Neretnieks, I. (2017). Solute transport in channel networks with radial diffusion from channels in a porous rock matrix. Swedish Nuclear Fuel and Waste Management Co, Report SKB R-15-02, 32 pp.

Nicolas, A., & Poirier, J.-P. (1976). *Crystalline plasticity and solid state flow in metamorphic rocks*. Wiley.

Oppermann, R. (1990). Mikrothermometrie- und Kathodolumineszenz-Untersuchungen an Quarzen des Bayerischen Pfahls. Unpublished Diploma Thesis, Georg-August-Universität zu Göttingen.

Peck, D. L., Hamilton, M. S., & Shaw, H. R. (1977). Numerical analysis of lava lake cooling models: Part II, application to Alae Lava Lake, Hawaii. *American Journal of Science*, *277*(4), 415–437. https://doi.org/10.2475/ajs.277.4.415

Peucker-Ehrenbrink, B., & Behr, H.-J. (1993). Chemistry of hydrothermal quartz in the post-Variscan "Bavarian Pfahl" system, F.R. Germany. *Chemical Geology*, *103*(1–4), 85–102. https://doi.org/10.1016/0009-2541(93)90293-R

Plümper, O., Botan, A., Los, C., Liu, Y., Malthe-Sørenssen, A., & Jamtveit, B. (2017). Fluid-driven metamorphism of the continental crust governed by nanoscale fluid flow. *Nature Geoscience*, *10*, 685–690. https://doi.org/10.1038/NGEO3009

Price, J. D., Wark, D. A., Watson, E. B., & Smith, A. M. (2006). Grain-scale permeabilities of faceted polycrystalline aggregates. *Geofluids*, *6*(4), 302–318. https://doi.org/10.1111/j.1468-8123.2006.00149.x

Putnis, A., & Austrheim, H. (2013). Mechanisms of metasomatism and metamorphism on the local mineral scale: The role of dissolution-reprecipitation during mineral re-equilibration. In D.E. Harlov and H. Austrheim (Eds.), *Metasomatism and the chemical transformation of rock* (pp. 141-170). Lecture Notes in Earth System Sciences. Springer. https://doi.org/10.1007/978-3-642-28394-9_5

Raghami, E., Schrank, C., & Kruhl, J. H. (2020). 3D modelling of the effect of thermal-elastic stress on grain-boundary opening in quartz grain aggregates. *Tectonophysics*, *774*, 228242. https://doi.org/10.1016/j.tecto.2019.228242

Schaarschmidt, A., Haase, K. M., de Wall, H., Bestmann, M., Krumm, S., & Regelous, M. (2019). Upper crustal fluids in a large fault system: Microstructural, trace element and oxygen isotrope study on multi-phase vein quartz at the Bavarian Pfahl, SE Germany. *International Journal of Earth Sciences*, *108*, 521–543. https://doi.org/10.1007/s00531-018-1666-y

Schenk, O., & Urai, J. L. (2004). Microstructural evolution and grain boundary structure during static recrystallization in synthetic polycrystals of sodium chloride containing saturated brine. *Contributions to Mineralogy and Petrology*, *146*(6), 671–682. https://doi.org/10.1007/s00410-003-0522-6

Schenk, V. (1989). P-T-t paths of the lower crust in the Hercynian fold belt of southern Calabria. In J. S. Daly, R. A. Cliff, & B. W. D. Yardley (Eds.), *Evolution of metamorphic belts*. *Geological Society of London Special Publications*, *43*, 337–342.

Schreiner, A. (1984). *Hegau und westlicher Bodensee. Sammlung Geologischer Führer, 62*. Borntraeger, 93 pp.

Segnit, E. R., Holland, H. D., & Biscardi, C. J. (1962). The solubility of calcite in aqueous solutions – I The solubility of calcite in water between 75° and 200° at CO_2 pressures up to 60 atm. *Geochimica Cosmochimica Acta*, *26*(12), 1301–1331. https://doi.org/10.1016/0016-7037(62)90057-1

Shimizu, H., Fukuda, J., Muto, J., & Okudaira, T. (2017). Reaction induced grain boundary cracking and anisotropic fluid flow during prograde devolatilization reactions within subduction zones. *Contributions to Mineralogy and Petrology*, *172*(9), 75. https://doi.org/10.1007/s00410-017-1393-6

Skinner, B. J., & Porter, S. C. (1989). *The dynamic earth*. John Wiley, 541 pp.

Stipp, M., Stünitz, H., Heilbronner, R., & Schmid, S. M. (2002). The eastern Tonale fault zone: A 'natural laboratory' for crystal plastic deformation of quartz over a temperature range from 250 to 700 °C. *Journal of Structural Geology*, *24*(12), 1861–1884. https://doi.org/10.1016/S0191-8141(02)00035-4

Stöckhert, B., Brix, M. R., Kleinschrodt, R., Hurford, A. J., & Wirth, R. (1999). Thermochronometry and microstructures of quartz – A comparison with experimental flow laws and predictions on the temperature of the brittle-plastic transition. *Journal of Structural Geology*, *21*, 351–369. https://doi.org/10.1016/S0191-8141(98)00114-X

Su, W., Xu, S., Jiang, L., & Liu, Y. (1996). Coesite from quartz jadeitite in the Dabie Mountains, Eastern China. *Mineralogical Magazine*, *60*(4), 659–662. https://doi.org/10.1180/minmag.1996.060.401.12

Taetz, S., John, T., Bröcker, M., Spandler, C., & Stracke, A. (2018). Fast intraslab fluid-flow events linked to pulses of high pore fluid pressure at the subducted plate interface. *Earth and Planetary Science Letters*, *482*, 33–43. https://doi.org/10.1016/j.epsl.2017.10.044

Taylor, D. (1972). The thermal expansion behaviour of the framework silicates. *Mineralogical Magazine*, *38*, 593–604. https://doi.org/10.1180/minmag.1972.038.297.08

Tullis, J. (1983). Deformation of feldspars. *Reviews in Mineralogy*, *2*, 297–323.

Vernon, R. H. (2004). *A practical guide to rock microstructure*. Cambridge University Press, 594 pp.

Voll, G. (1960). New work on petrofabrics. *Liverpool and Manchester Geological Journal*, *2*, 503–567.

Voll, G. (1969). Klastische Mineralien aus den Sedimentserien der Schottischen Highlands und ihr Schicksal bei aufsteigender Regional- und Kontaktmetamorphose. Habilitationsschrift, Fakultät für Bergbau und Hüttenwesen. *Technische Universität Berlin*, *D83*, 27 ff.

Voll, G. (1976). Recrystallization of quartz, biotite and feldspars from Erstfeld to the Leventina Nappe, Swiss Alps, and its geological significance. *Schweizerische Mineralogische und Petrographische Mitteilungen*, *56*, 641–647.

Watson, E. B., & Brenan, J. M. (1987). Fluids in the lithosphere, 1. Experimentally-determined wetting characteristics of CO_2-H_2O fluids and their implications for fluid transport, host-rock physical properties, and fluid inclusion formation. *Earth and Planetary Science Letters*, *85*, 497–515. https://doi.org/10.1016/0012-821X(87)90144-0

Wilson, J. L., Evans, L., & Delle Piane, C. (2009). Modelling of porphyroclasts in simple shear and the role of stress variations at grain boundaries. *Journal of Structural Geology*, *31*(11), 1350–1364. https://doi.org/10.1016/j.jsg.2009.08.001

Yardley, B. W. D. (1989). *An introduction to metamorphic petrology*. Longman Group, 248 pp.

Yardley, B. W. D. (2013). The chemical composition of metasomatic fluids in the crust. In D. E. Harlov, & H. Austrheim (Eds.), *Metasomatism and the chemical transformation of rock* (pp. 17–51). Lecture Notes in Earth System Sciences. Springer. https://doi.org/10.1007/978-3-642-28394-9_2

Yilmaz, T. I., Prosser, G., Liotta, D., Kruhl, J. H., & Gilg, H. A. (2014). Repeated hydrothermal quartz crystallization and cataclasis in the Bavarian Pfahl shear zone (Germany). *Journal of Structural Geology*, *68A*, 158–174. https://doi.org/10.1016/j.jsg.2014.09.004

SUPPORTING INFORMATION

Additional supporting information may be found online in the Supporting Information section.

Figure S1: HAADF TEM image of a partially filled albite–amphibole phase boundary and of a fracture in amphibole (see Figure 5a for comparison) and semi-quantitative EDX measurements within outlined areas in the filled boundary (area 1) and in amphibole (area 2).

Figure S2: Semi-quantitative EDX analyses of magmatic amphibole (area 2) and amphibole newly grown in the open phase boundary (area 1).

Figure S3: HAADF TEM image of two amphibole grains and their boundary, which is straight and completely filled with sheet silicate.

Figure S4: HAADF TEM image and semi-quantitative TEM EDX analyses of two clinopyroxene grains (areas 1 and 4) and their roughly 500 nm wide, filled boundary. See Figure 8 for details. The boundary is filled with sheet silicate (probably vermiculite) (area 2) and amorphous matter (area 3). Felsic granulite of the lowermost exposed part of the fossil Variscan lower continental crust of Calabria (southern Italy); sample KR3434B, foil 4835.

Video S1: This video of the 3D geometry of three grain boundaries in Carrara marble (~10 μm across) documents how the locations of the grain boundaries change in 3D and how the grain boundaries open and close even on the nanometre scale.

Table S1: Characteristics of analysed grain and phase boundaries as well as cracks and a cleavage plane.

Table S2: Basic data and calculation scheme for grain-boundary and dissolution-cavity porosity of the seven analysed rock samples.

How to cite this article: Wirth R, Kruhl JH, Morales LFG, Schreiber A. Partially open grain and phase boundaries as fluid pathways in metamorphic and magmatic rocks. *J Metamorph Geol*. 2022;40:67–85. https://doi.org/10.1111/jmg.12610